EUROPEAN ORGANIZATION FOR NUCLEAR RESEARCH
European Laboratory for Particle Physics

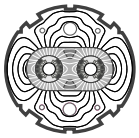

Large Hadron Collider Project

LHC PROJECT REPORT 176

Design Features and Performance of a 10 T Twin Aperture Model Dipole for LHC

D. Leroy, L. Oberli, D. Perini, A. Siemko, G. Spigo

Abstract

A twin-aperture superconducting (sc) dipole model has been designed in collaboration with Finnish and Swedish Institutions and built at CERN. The cable critical current was attained at a central field of 10.5 T at a temperature of 1.77 K after three training quenches only. This model has shown a very good quench performance as well as a robust mechanical behaviour over several thermal cycles. This paper will discuss the design, the innovations of the mechanical structure, and the results obtained during the intensive campaigns of tests.

LHC Division

Presented at the 15th International Conference on Magnet Technology (MT15), Beijing, China, October 1997

Administrative Secretariat
LHC Division
CERN
CH 1211 Geneva 23

Geneva, 14 May 1998

Design Features and Performance of a 10 T Twin Aperture Model Dipole for LHC

D. Leroy, L. Oberli, D. Perini, A. Siemko, G. Spigo

CERN, European Organization for Nuclear Research - 1211 Geneva 23, Switzerland

***Abstract* — A twin-aperture superconducting (sc) dipole model has been designed in collaboration with Finnish and Swedish Institutions and built at CERN. The cable critical current was attained at a central field of 10.5 T at a temperature of 1.77 K after three training quenches only. This model has shown a very good quench performance as well as a robust mechanical behaviour over several thermal cycles. This paper will discuss the design, the innovations of the mechanical structure, and the results obtained during the intensive campaigns of tests.**

I. Introduction

Despite the LHC nominal beam energy of 7 TeV is obtained with a magnetic central field of 8.36 T, the R & D program, exploring the maximum attainable fields, was mantained to investigate and verify the performance of different designs and manufacturing procedures. Within the framework of the R & D program for LHC dipoles, a twin-aperture model magnet was built. This model has apertures of 56 mm and its main features are austenitic steel collars, separate collared coils and a closed yoke gap at room temperature. A collaboration was established with the Helsinki University of Technology (Finland), the Uppsala University (Sweden) and CERN to design and build the twin-aperture-model dipole called MFISC. Its fabrication was carried out at CERN and ended in June 1995. The overall design and the details of the fabrication were presented in previous papers [1], [2], [3]. Three campaigns of tests took place at CERN. Between each run the magnet was warmed up and kept at room temperature for some time. In the first campaign (July 1995) the short sample limit of 10.5 T central field, that corresponds to a 10.95 T peak field in the inner cable, was reached after three training quenches. In the second (August 1995) and the third campaign (November 1996) the magnet had its first quench at fields close to cable short sample limit. This report will describe the mechanical concepts, the choice of materials and the experimental results.

II. Description of the Magnet

The aperture and the overall length of the magnet are 56 mm and 1.3 m respectively. The 16.7 mm wide NbTi sc cables have different trapezoidal shapes and thicknesses to adapt the current density to the maximum magnetic field in the coils and to obtain a correct conductor placement on the circular winding mandrel for good field quality. The working temperature of the magnet is that of superfluid helium ($T < 2.16$ K). The main parameters of the dipole are summarized in Table I and the magnet cross section is shown in Fig. 1. The centering and alignment of the collared coil in the yoke structure is realized by means of collar bulges which are clipped in special grooves made in the yoke. The yoke is vertically split and composed of three pieces. At all times, the yoke gap is closed and the contact between the collared coil and the yoke is extended over an angle of ± 60 degree.

TABLE I
Model dipole parameters

Coil turns per beam channel		
inner shell	28	
outer shell	54	
Reference field	10	T
Stored energy for both channels	760	kJ/m
Current at reference field	14370	A
Self-inductance for both channels	7.35	mH/m
Coil aperture diameter	56	mm
Magnetic length	840	mm
Iron length	670	mm
Collared coil length	1080	mm
Overall length	1320	mm
Intra-beam distance	200	mm
Collar diameter	182	mm
Inner yoke diameter	183	mm
Outer diameter	600	mm
Resultant of e-magnetic forces in first coil quadrant		
$\sum Fx$	2.12	MN
$\sum Fy$	- 1.03	MN
Axial electro-magnetic force on magnet ends	760	kN

This angle is also the good compromise between the need of an easy assembly and the aim of a maximum rigidity of the collared coil.

At room temperature, the yoke pieces are maintained around the collared coils with a force of about 400 kN/m after the welding of the 10-mm-thick austenic steel cylinder. During cooldown, due to the greater integrated coefficient of thermal expansion of the austenitic steel with respect to the that of the iron (closed gap), this force doubles and reaches a value close to 800 kN/m. The assembly permits a good transmission of the horizontal component of the magnetic forces which implies negligible collared coil deformations due to bending and then an improved magnetic field quality.

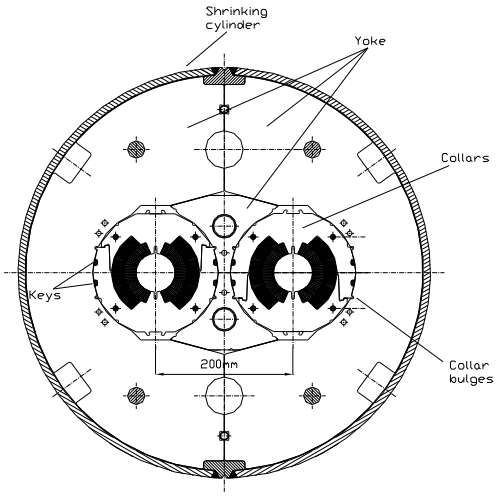

Fig. 1. Cross Section of the Magnet Model

III. The Superconducting Cable

The strand material is a Nb47Ti/Cu composite with 5 μm diameter filaments. The main cable parameters are listed in Table II. Both type of strands have a 1 μm thick Sn5Ag coating. To avoid sharp edges on the thin side of the cables, the compaction ratio (91%) has been decreased with respect to that adopted for the previous 50 mm aperture LHC superconducting dipole magnets.

Critical current measurements made on strands extracted from cables indicate that cable degradation is lower than 3 %. The average value of the measured interstrand resistance R_c is 16 μΩ [4]. This value is above the minimum target of 10 μΩ that is needed to limit the degradation of the magnetic field quality due to dynamic distortions.

TABLE II
CHARACTERISTIC DATA OF THE CABLE

	INNER LAYER	OUTER LAYER
Diameter of strand (mm)	1.1	0.87
Cu/Sc ratio	1.6	1.87
Filament size (μm)	5	5
J_c at 8 T and 4.2 K (A/mm^2)	1070	1108
Number of strands	30	38
Mid thickness bare (mm)	1.965	1.560
Width bare (mm)	16.7	16.7
Keystone angle	1.20	0.83
Number of filaments	20328	9438
dJ_c/dB (A/mm^2/T)	487	609

IV. Mechanical Structure Optimisation

A. Cross Section Basic Principles

The cross section of a superconducting magnet has to fulfil two basic needs: good mechanics, and good magnetic field quality. These requirements can be met in different ways that lead to different magnet designs. In our case, the design is based on the two following concepts:

1) *extended-line-to-line fit*: at any stage, the outer radius of the collar is the same as the inner radius of the iron yoke, and

2) *enlarged-yoke-to-yoke contact*: at any stage, the mating faces between the three yoke pieces are under compression.

The enlarged-yoke-to-yoke contact concept relies on the particular distribution of the force of the cylinder among the different yoke pieces, thus, resulting in an increase of cold-mass overall rigidity. The extended-line-to-line-fit design relies on the large contact perimeter between the collared coils and the closed iron yoke that defines a clear circular boundary which is needed to ensure good magnetic field quality. The taper of the central yoke piece permits the use of a parallel gap during assembly. This rigid support also helps confine any collared coil transition region (ramp splice and coil ends) in which the coil prestress is set up with less precision.

1) Collars: In any dipole magnet, the horizontal component of the magnetic force tends to deflect the collared coil along its horizontal axis. This deflection is counteracted by the closed yoke that provides an extremely stiff support which also preserves the circular shape of the collared coil. As the gap is already closed at room temperature, the good matching between yoke and collars, before excitation, depends on the choice of the collar material (coefficient of thermal expansion). Two opposite needs were to be minimized: 1) the loss of coil azimuthal prestress, and 2) the loss of contact between yoke and collars. The best compromize was reached by choosing an austenic steel with an integrated coefficient of thermal expansion between 300 K and 2 K of 2.7 x 10^{-3} compared to that of the coil (5.2 x 10^{-3}) and that of the yoke (2.0 x 10^{-3}). As the integrated coil coefficient of thermal expansion is greater than that of collars, the different shrinkages help homogenize local coil stress disturbancies. The collars should be flexible enough to limit the tendency to build up shear and bending stresses in the coils during manufacturing (i.d. collaring and yoking) and to adapt their external shape to the yoke inner circumference. Moreover, since the yoke is vertically split, the vertical deformation of the collared coil has to be limited to allow its easy assembly in the yoke. By playing with the collar width and, therefore, with the collar neutral axis, the most advantageous compromize can be found. In our case, the collared coil vertical spring constant is 12.6 GN/m per unit of length and the ratio between the collar neutral axis and the collar width is close to 3. By doing so, the collared coil horizontal spring constant is also fixed and is about half of the vertical one. The elliptical shape of the collared coil, after collaring, was limited to 120-130 μm (radial vertical displacement) to be assembled with an interference of 90 ± 10 μm and a ± 60-degree contact in the yoke cavity. Due to the ± 60-degree line-to-line fit, the collared coil horizontal spring constant increases more than four times. This rise of the collared coil rigidity was considered sufficient for the good mechanical behaviour of the structure compared to the rigidity of the usual ± 15 to 20 degree fit. Table III summarizes the rigidities and maximum bending moments of the collared coil (modelled as a ring) for the same horizontal integrated force distributed over different angles of contact.

2) Yoke: The yoke pieces are assembled around the collared coils and surrounded by two 10 mm thick austenitic steel half cylinders: a gap is then set between the two half-yokes. This assembly is slid into the press and compressed until the chamfers of the two half shells reach the value required to weld the external cylinder. After assembly, the yoke gap is closed, the coils are further compressed azimuthally, and the collar and yoke circumferences fit perfectly. To obtain the most rigid support for the collared coil and stabilize the whole mechanical structure, the yoke pieces were shaped so that a large vertical force could be transmitted from the austenic steel shrinking cylinder to the 15-degree-tapered yoke central piece by means of the two yoke halves (enlarged-yoke-to-yoke contact). In this way, during excitation, the loss of the yoke mating force between the two yoke halves is greatly reduced. Since the collared coil and the yoke fit perfectly, the horizontal component of the magnetic forces is directly transferred from coils to yoke. The quasi-infinite rigid boundary (around 100 GN/m per unit of length) seen by the collared coil prevents the coils from moving radially. This implies that the geometry of the coils is negligeably modified during energization.

3) Yoke-Collared Coil Contact: During cooldown, the different parts of the cold mass shrink with different integrated coefficients of thermal expansion and slide among each other on their common interfaces thanks to the presence of sliding low friction sheets (coil-to-collars and collars-to-yoke) [2].

TABLE III
COLLARED COIL RIGIDITIES AND BENDING MOMENTS
(RATIO BETWEEN THE ACTUAL VALUE AND THE VALUE ZERO DEGREE)

ANGLE	INCREASE OF RIGIDITY	BENDING MOMENT
0	1	1
30	2.4	0.629
60	4.3	0.303
90	13.5	0

TABLE IV

AVERAGE COIL LAYER AZIMUTHAL STRESS HISTORY (MPa)

	293 K	2 K	2 K at 9 T
INNER	70	45	~ 0
OUTER	70	45	7

As a result, stresses coming from bending, induced by relative movements, are negligible or completely absent. Since the collared coil is assembled with interference, its shape remains round and always fits the yoke inner circumference. This means that there is no change of the collar horizontal spring constant between warm and cold conditions, even though the thermal shrinkage differentials result in changes of coil azimuthal stress and collared coil shape. The combined effect of low-friction-coil-to-collars interface and the quasi-infinite rigid boundary entails that the coils are unloaded essentially by the azimuthal compressive component of the magnetic force. The absence of undesired bending moments permits lowering the load that is needed to hold the prestressed coil against the collar pole at maximum current. In fact, if the collared coil is modelled as a thick-wall tube submitted to an external pressure (reaction of the yoke inner shape against the magnetic force) the coils can see, during excitation, an increase of azimuthal stress from the outer to the inner radius of the coil (stress gradient). In this case, the outer edge of the coil may start unloading while the inner edge remains fully loaded. This partial loading is sufficient to prevent the conductors from moving and to obtain good quench performance even if the measured average coil azimuthal stress appears to be close to zero. Table IV summarizes the pole average azimuthal stresses measured in the inner and outer layer of the coils at various stages of fabrication and excitation.

B. Longitudinal Section

Training quenches are often observed in sections close to the ends. This is due to two main reasons: magnetics (high field gradient), mechanics (different azimuthal compressive stresses between ends and straight part). To partially overcome this problem a threefold approach was considered: 1) reduced longitudinal field gradient (dB/dz) by the magnetic design of the ends 2) low prestress in the ends and minimum stress gradient ($d\sigma_\theta/dz$) in zones between ends and straight part, and 3) compaction of the coil ends (*cage*). The cross sectional view of the "*cage*" [2] is shown in Fig. 2.

V. Performance of the Magnet

The magnet was tested in a vertical cryostat in which the temperature of the superfluid helium could be adjusted between 1.7 and 2.1 K. Three campaigns of tests took place and the quench history is shown in Fig. 3. In the first campaign, the first quench occured at a central field of 8.91 T at a temperature of 1.9 K and after three more training quenches (9.53 T, 10.06 T, 10.2 T), the magnet attained its short sample limit (10.42 T at 1.9 K). At 4.42 K, the quenching field was 7.82 T, measured at the end of the test run. The magnet was then warmed up and two weeks later cooled down again. In the second campaign, the magnet had two training quenches at high field (10.04 T, 10.06 T) before reaching the short sample limit.

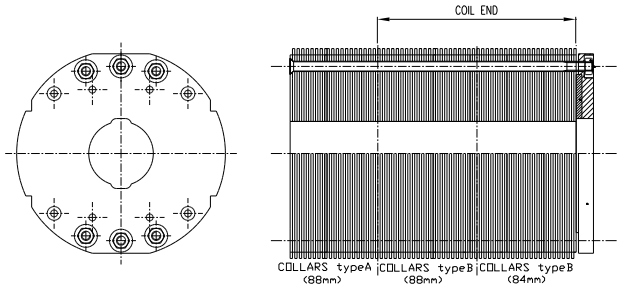

Fig. 2. Cross Sectional View of the "Cage"

The third run took place more than one year later and the magnet had one training quench only (10.1 T) before reaching again the short sample limit. As expected, all highest field quenches were located in the straight part since they are at the short sample limit. To extrapolate the cable short sample field limit, some quenches were performed at a ramp rate of 0 A/s (plateau current at a given magnetic field) letting the superfluid helium bath warm up. The experimental fit is shown in Fig. 4. The data indicate that all highest field quenches reached by the magnet lie on the critical current-limitation line and are truly short sample limit ones. In the first two campaigns about two third of the magnetic energy was extracted while in the last the whole energy was dissipated in the magnet by delaying the switching of the dump resistor. The maximum temperature of the hot spot reached by the conductor (outer coil layer), deduced by the MIITs curve, was about 240 K (37 MIITs). During the first excitation, a large number of "*spikes*" (sharp increase of coil voltage) were observed at fields lower than 8.91 T (first quench) but did not trigger any quench. Later on, these disturbances were not observed anymore.

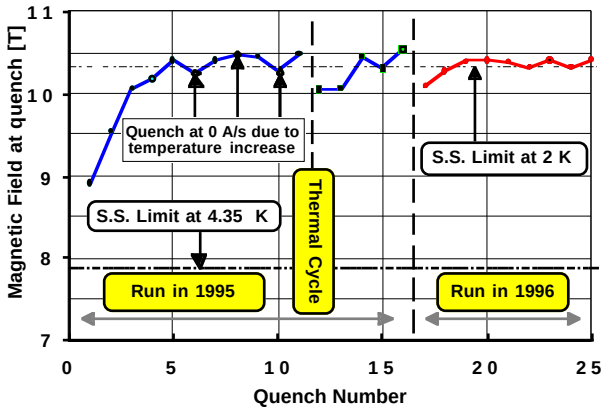

Fig. 3. Quench History

Due to the sufficiently high value of the interstand resistance R_c, the magnet showed a satisfactory ramp rate sensitivity. In fact, the magnet reached short sample limit at a ramp rate of 50 A/s which is well above the ramp rate foreseen during the operation of the LHC machine (10 A/s).

VI. Magnetic Results

The quality of field, along the longitudinal axis, is measured using rotating harmonic coils. The multipoles are shown in Table V. The large positive normal sextupole component with respect to the computed one (3 units) is explained by the smaller azimuthal coil size dimensions measured during manufacturing. As already mentioned, the horizontal component of the magnetic force produces a deflection of the collared coil along the mid-plane. If the collared coil is free to deflect outwards, a negative sextupole occurs. On the other hand, if the collared coil does not deflect and the coil conductors always touch the collar pole, the sextupole component is constant. In our case, as shown in Fig. 5, the measured sextupole components versus current exhibits no change, even after several thermal cycles. This is a strong and independent indication that, during energization, the collared coil does not move and the coils are sufficiently loaded to prevent the conductors from moving.

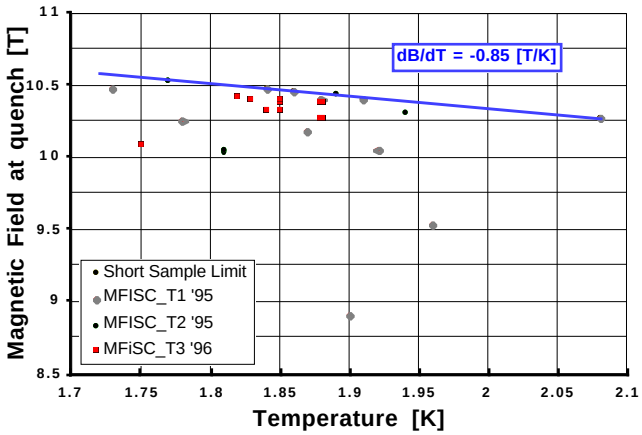

Fig. 4. Quench Field versus Temperature

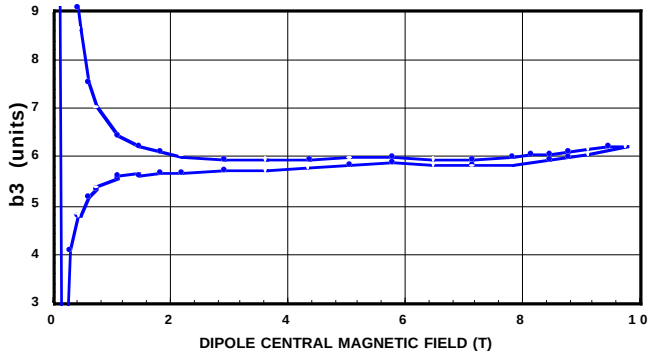

Fig. 5. - Measured Average Normal Sextupole Component (Mid Section)

TABLE V

MEASURED NORMAL AND SKEW GEOMETRICAL MULTIPOLE COMPONENTS (IN UNITS OF 10^{-4} RELATIVE FIELD ERROR AT 10 mm)

	0.66 T MAGNETIC FIELD		9 T MAGNETIC FIELD	
n	norm b_n	skew a_n	norm b_n	skew a_n
2	0.226	0.488	1.011	0.719
3	7.256	- 0.25	7.004	- 0.43
4	- 0.038	0.175	0.022	0.014
5	0.038	0.058	0.045	0.016
6	- 0.0103	- 0.0205	- 0.0102	- 0.0002
7	0.0425	- 0.02	0.0332	- 0.0075
8	0.002	0.0028	0.0017	0.001
9	0.00017	0.0007	- 0.0004	0.0002
10	0.0018	- 0.003	0.0017	- 0.0034
11	0.0053	- 0.0017	0.0057	- 0.0024

VII. Conclusion

The MFISC magnet reached the short sample limit of 10.5 T with minimum training and with almost no retraining in the successive test campaigns. This excellent quench performance demonstrates that the structure is not yet mechanically limited and proves the soundness and validity of the concepts of the extended line-to-line fit and the enlarged yoke-to-yoke contact. It is worth noting that it is the first time that magnetic fields greater than 10 T are attained at 1.9 K with a very small training similar to the one observed in the best accelerator magnets working at 4.2 K.

Acknowledgment

The authors wish to thank for their continuous support E. Bycking (Helsinki University of Technology), T. Ekelöf (Uppsala University) and R. Perin (CERN) who promoted this collaboration. Also, many thanks to N. Dalexandro, P. Geroudet, H. Kummer, G. Trachez and L. Walckiers for their assistance during the construction and the tests of the magnet.

References

[1] J. Ahlbäck et al., "Electromagnetic and Mechanical Design of a 56 mm Aperture Model Dipole for the LHC", IEEE Trans. on Magnetics, July 1994, vol 30, No. IV, pp. 1746-1749

[2] J. Ahlbäck et al., "Construction of a 56 mm Aperture High-Field Twin-Aperture Superconducting Dipole Model Magnet", IEEE Trans. on Magnetics, July 1996, vol 32, No. IV, pp. 2097-2100

[3] M. Savalainen, "MFISC Iron Circuit", AT-MA Internal Note 93-85, June 1993

[4] D. Richter et al., “DC Measurement of Electrical Contacts between Strands in Superconducting Cables for the LHC Main Magnets”, IEEE Trans. on Applied Superconductivity, June 1997, vol 7, No II pp. 786-792

[5] L. Bottura, “Results of Magnetic Measurements on the MFISC Model Dipole”, CERN AT-MA Technical Note 95-105, September 1995